



Contents lists available at ScienceDirect

Marine and Petroleum Geology

journal homepage: www.elsevier.com/locate/marpetgeo

Research paper

A late Miocene–Early Pliocene biogenic silica crash in the Andaman Sea and Bay of Bengal

T. Cawthern ^{a,*}, J.E. Johnson ^a, L. Giosan ^b, J.A. Flores ^c, K. Rose ^d, E. Solomon ^e^a Department of Earth Sciences, University of New Hampshire, Durham, NH 03824, USA^b Department of Geology and Geophysics, Woods Hole Oceanographic Institute, Woods Hole, MA 02543, USA^c Grupo de Geociencias Oceanicas, Universidad de Salamanca, Salamanca, 37008, Spain^d National Energy Technology Laboratory, U.S. Department of Energy, Albany, OR 97321, USA^e School of Oceanography, University of Washington, Seattle, WA 98195-7940, USA

ARTICLE INFO

Article history:

Received 2 December 2013

Received in revised form

22 July 2014

Accepted 26 July 2014

Available online xxx

Keywords:

Indian Ocean

Bay of Bengal

Indonesian Throughflow

NGHP-01

Biosilica

ABSTRACT

Variations in the mass accumulation rate of biogenic silica (BSi) in continental margin sediments can be used to reconstruct relative changes in productivity through time in these settings. In the northern Bay of Bengal a lack of long sedimentary records has historically precluded this type of reconstruction. The acquisition of 21 new long sedimentary records during the 2006 Indian National Gas Hydrate Program (NGHP) Expedition-01 has made it possible for the first time to reconstruct paleoproductivity in this important region of the world that is dominated by intense changes in the geological and biological fluxes largely driven by tectonic and climate related mechanisms. In the research presented here, fluctuations in the mass accumulation rate of biogenic opal during the past ~9.4 Myrs are reconstructed using continental margin sediment cores from the Andaman Sea (Site NGHP-01-17A) and the northern Bay of Bengal (Site NGHP-01-19). Within these records, a biogenic silica crash is recorded at ~6 Ma and is consistent with previous geotectonic, geochemical and paleontological studies of the southern Indian Ocean and Pacific Ocean that suggest connectivity, and thus exchange of nutrient-rich water masses, between the eastern tropical Indian Ocean and western tropical Pacific Ocean was diminished as a result of the tectonic restriction of the northerly sector of the Indonesian Throughflow (ITF). The biogenic silica crash at Sites 17 and 19 is consistent with a decrease in surface water productivity that may have been driven by the reduction of nutrient-rich Pacific waters delivered to the Andaman Sea and Bay of Bengal via the northerly route of the ITF. Following the BSi crash at ~6 Ma, subsequent recovery of the BSi mass accumulation rates at Sites 17 and 19 occurred and was perhaps renewed by an enhanced supply of nutrient-rich freshwater from the nearby Irrawaddy and Mahanadi Rivers, which could have occurred during a documented increase in the intensity of the Indian monsoon at ~5 Ma. Although recovery is noted at both core locations, biogenic silica mass accumulation rates did not fully recover in the Andaman Sea. This could be explained by the restricted nature of the Andaman basin and its more distal location from a major source of nutrient-rich freshwater.

© 2014 Elsevier Ltd. All rights reserved.

1. Introduction

Several DSDP and ODP expeditions in the Pacific and north-central Indian Oceans have documented significant increases in the mass accumulation rates (MAR) of biogenic sediments during

the late Miocene–Pliocene (e.g., Leinen, 1979; Woodruff, 1985; Farrell et al., 1995; Dickens and Owen, 1996). These changes mark important shifts in planktonic and benthic productivity, and are especially well developed in oceanographic divergence zones (Peterson et al., 1992; Berger et al., 1993; Dickens and Owen, 1994). The time-coincident nature of biogenic sediment increases in the Pacific and Indian Oceans resulted in the development of the “biogenic bloom” hypothesis that suggests enhanced nutrient upwelling to surface waters in divergence zones led to an increase in the downward flux of biogenic sediments and an expansion of the oxygen minimum zone, enhancing preservation (e.g., Dickens and Owen, 1999). Sediment deposited between 9.0 and 3.5 Ma in

* Corresponding author. Department of Geography and Geosciences, 1101 Camden Ave., Salisbury University, Salisbury, MD 21801, USA. Tel.: +1 410 677 6514.

E-mail address: trcawthern@salisbury.edu (T. Cawthern).

¹ Now at Department of Geography and Geosciences, Salisbury University, Salisbury, MD 21801, USA.

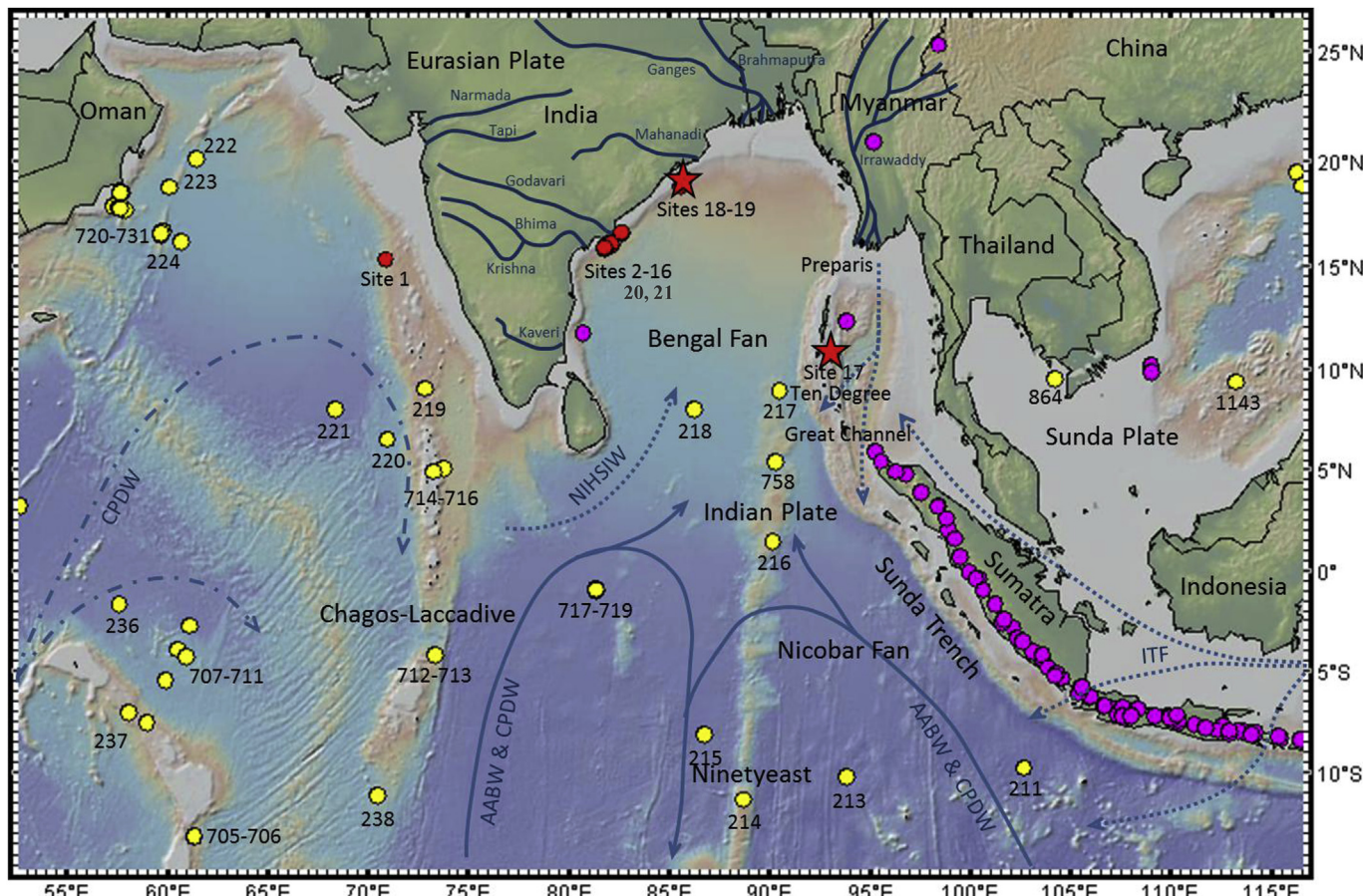
these ocean basins contain planktonic and benthic fauna that are indicative of high productivity and organic content and redox signatures indicative of low dissolved O₂ (Dickens and Owen, 1999).

Two potential mechanisms have been proposed to explain the origin of the late Miocene–Pliocene biogenic bloom: 1) elevated nutrient supply to the ocean basins via increased continental weathering or 2) a redistribution of nutrients within the oceans resulting from a change in the strength of deep water formation (Dickens and Owen, 1999) or an opening and closing of passages for ocean circulation (e.g., Keller and Barron, 1983; Cortese et al., 2004). Although both scenarios are plausible, a better understanding of the late Miocene–Pliocene biogenic bloom may be achieved as the spatial distribution of its occurrence and its timing are better constrained globally.

Although plausible explanations for the late Miocene–Pliocene biogenic bloom have been proposed and discussed, the subsequent cessation of the bloom has received limited discussion (Keller and Barron, 1983; Farrell et al., 1995; Dickens and Owen, 1999). In this paper, we document the biogenic silica mass accumulation rate (MAR) of sediments located in the Andaman accretionary wedge at National Gas Hydrate Program of India Expedition-01 (NGHP-01) Site 17 ($10^{\circ} 45.1912'N$, $93^{\circ} 6.7365'E$) and in the northwestern Bay of Bengal at NGHP-01 Site 19 ($18^{\circ} 58.6568'N$, $85^{\circ} 39.5202'E$) and discuss the mechanisms that may have caused an observed abrupt decrease or “crash” in BSi at ~6 Ma at both sites.

2. Geologic setting

The seafloor sedimentary record in the Bay of Bengal in the northern Indian Ocean is dominated by the Bengal and Nicobar submarine fans, which have received terrigenous sediments from the erosion of the Himalayan Mountains via transport through the Ganges–Brahmaputra drainage systems during the last 15 million years (Curry et al., 2003; Bastia et al., 2010, Fig. 1). The extent of the Bengal Fan is limited to the west by the continental shelf and slope of peninsular India, which formed as a passive margin during the break-up of Gondwana (Powell et al., 1988; Curry et al., 2003; Bastia et al., 2010) and has received terrigenous sediments from the modern Mahanadi, Krishna, Godavari and Kaveri Rivers and predecessor rivers (Fig. 1). Site 19 is located on the slope, above the modern-day depocenter of the Bengal Fan, on the eastern margin of peninsular India, just south of the Mahanadi River discharge. To the east, across the Bay of Bengal, much of the Bengal Fan has been subducted or accreted beneath the Sunda Subduction Zone (Bowles et al., 1978; Curry et al., 2003). As the aseismic Ninety East Ridge continues to approach the subduction zone it also inhibits Bengal Fan sedimentation, isolating the more westerly and previously deposited fan sediments, now known as the Nicobar Fan, from the main Bengal Fan lobe (Bowles et al., 1978; Curry et al., 2003). Farther to the east, the semi-enclosed Andaman Sea is located in a back-arc basin formed by the oblique subduction of the Indian Plate beneath the Sunda Plate (Rodolfo, 1969; Karig et al., 1980; Pal et al.,



2003; Raju et al., 2007). Backarc extension and the concomitant formation of the Andaman Sea began between 11 and 4 Ma (Rodolfo, 1969; Karig et al., 1980; Pal et al., 2003; Raju et al., 2007). Since ~4 Ma, active backarc spreading in the Andaman Sea has resulted in total extension of ~460 km (Raju et al., 2004; Khan and Chakraborty, 2005). Within the Andaman Sea, terrigenous sediments from the Irrawaddy River are deposited on the shelf and slope, north of the Andaman back-arc spreading center (Rodolfo, 1975). Transportation of fine-grained sediments are restricted to the nearshore region by monsoonal surface currents (Rodolfo, 1975; Babu et al., 2010; Tripathy et al., 2011). Site 17 is located in the Andaman accretionary wedge, east of Little Andaman Island. Both Sites 17 and 19 are located at depths above the reach of sediment gravity flows associated with the Bengal Fan and thus preserve nearly continuous records of pelagic/hemipelagic sedimentation that are ideal for paleoceanographic study.

3. Site and core stratigraphy

This study focuses on the stratigraphic records recovered from two marine sedimentary records from the northeast Indian Ocean. Site 17 was drilled in the Andaman accretionary wedge, east of Little Andaman Island in the Andaman Sea (Fig. 1). This site is located in 1344 m of water, far from major sources of terrestrial clastic influx, and preserves predominantly carbonate oozes with intervals rich in biogenic silica, within fine-grained (clay-sized) terrigenous material, punctuated by volcanic ashes (Collett et al., 2008; Rose et al., 2014). Site 19 was drilled in the Mahanadi Basin, located along the eastern passive continental margin of India proximal to the mouth of the Mahanadi River. Site 19 is located in 1422 m of water and is the most heterolithic core from NGHP Expedition-01 (Collett et al., 2008). The hemipelagic record at Site 19 consists of varying amounts of silt and clay sized minerals, volcanic glass, pyrite, authigenic carbonate and aragonite, plant debris, nannofossils, biogenic silica and foraminifera (Collett et al., 2008; Phillips et al., 2014).

Shipboard smear slide and coarse fraction analyses of the sediments at Site 17 indicate a shift in the marine microfossils occurred since the late Miocene (Collett et al., 2008). Specifically, biosiliceous and carbonate marine fossils dominate the lower half of the core, whereas carbonate-bearing marine fossils dominate the upper half of the core (Fig. 2). The record recovered from Site 19 also follows the same pattern in biogenic components (Fig. 2).

The ages of the records at Sites 17 and 19 were determined using a detailed nannofossil age model (Fig. 3). Calcareous nannofossil events were identified at Sites 17 and 19 spanning an interval from the Pleistocene to the middle Miocene (Flores et al., 2014), based on standard biozones of Martini (1971) and Okada and Bukry (1980). The biochronology was developed following Raffi and Flores (1995) and Raffi et al. (2006) using astronomically calibrated ages from magnetic reversals and reference isotope stratigraphies.

4. Oceanographic setting

In the Indian Ocean, intermediate and deep water masses originate from the Atlantic and Southern Oceans (Fig. 1). Intermediate waters (~1200–3800 m) are comprised of a mixture of Antarctic Bottom Water (AABW) and North Atlantic Deep Water (NADW) (also known as Circumpolar Deep Water, CPDW) (Vincent, 1974; Kawagata et al., 2006). Deep waters (>3800 m) are formed from northward-flowing cold, well-oxidized Antarctic Bottom Water (AABW) (Peterson, 1984; Kawagata et al., 2006). Within the Bay of Bengal, the upper ~1000 m of the water column is bathed in North Indian High Salinity Intermediate Water (NIHSIW) and a seasonally-influenced low salinity surface water mass. The NIHSIW

enters the Bay of Bengal from the Arabian Sea as the Monsoon Current, but is ultimately derived from the Red Sea and Persian Gulf (Fig. 1; Murthy et al., 1992; Naqvi et al., 1994; Kawagata et al., 2006). The NIHSIW and low salinity surface water masses in the Bay of Bengal are highly dependent on the intensity of the summer and winter monsoons (Varkey et al., 1996). Differential heating of the ocean during the winter monsoon, compared to the Indian sub-continent results in the establishment of a high-pressure system over the land that leads to an intensification of the northerly winds, and causes decreased precipitation over the land and an increase in sea surface temperature in the Bay of Bengal (Varkey et al., 1996). In contrast, the summer monsoon results in the intensification of southerly winds that forces moisture-laden air originated from the Bay of Bengal over the Himalaya–Tibetan mountain range, and causes increased rainfall and freshwater discharge into the Bay of Bengal (Varkey et al., 1996). The major implication of the Asian monsoon and its intensity through time is the effect it has on the seasonal winds, precipitation, and run-off patterns, which affect the volume and composition of run-off entering the marginal seas. Increased precipitation and river runoff during the summer monsoon restricts vertical mixing and upwelling of deep nutrients to the photic zone proximal to the coast (e.g., Madhupratap et al., 2003; Prassana Kumar et al., 2002) in the Bay of Bengal and Andaman Sea. Another important influence of the monsoons is the seasonal variations they induce in temperature and density in the Bay of Bengal that results in very different circulation patterns. In particular, during the winter monsoon, surface water is transported clockwise in the Bay of Bengal, whereas during the summer monsoon, the direction of transport is reversed (Varkey et al., 1996). Upwelling-induced productivity in the Bay of Bengal and Andaman Sea regions is primarily located away from the continental margins, where the wedge of freshwater influx is thinner and wind stress is high, resulting in the formation of localized mesoscale cyclonic eddies (Wyrtki, 1961; Buranapratheprat et al., 2010; Rizal et al., 2012).

Deep, intermediate, and surface waters in the Andaman Sea are derived from freshwater runoff and the intermixing of water masses that originate from the Indian and Pacific Oceans (Ibrahim and Yanagi, 2006; Amiruddin et al., 2011). The Andaman–Nicobar Islands (located just west of Site 17) isolate most of the Andaman Sea deep waters from the Bay of Bengal deep waters in the northern sector of the Andaman Basin, but these two water masses intermix in the central Andaman Sea through the Preparis and Ten Degree Channel, and in the south through the Great Channel (Fig. 1; Varkey et al., 1996; Dutta et al., 2007). In contrast, intermediate and surface waters from the Bay of Bengal freely intermix with those of the Andaman Sea. Surface waters in the Andaman Sea are strongly affected by seasonal variations in the monsoons, particularly as a result of increased discharge of freshwater from the Irrawaddy, and Brahmaputra and Ganges Rivers (Fig. 1; Wyrtki, 1961; Rizal et al., 2012).

In addition to the seasonally-induced changes to the surface water within the Andaman Sea, studies from other ocean basins (i.e., Pacific) suggest that temporal variations in the connectivity of Indian and Pacific Ocean surface waters via the Indonesian Throughflow (ITF) has affected the productivity of carbonate (i.e., foraminifera) and biosiliceous plankton (i.e., diatoms and radiolarians) (Keller, 1985; Kennett et al., 1985; Romine and Lombari, 1985). The flow of Pacific Ocean waters westward into the Indian Ocean through the Indonesian archipelago and marginal seaways is the result of a pressure gradient that is established between the two ocean basins due to a difference in sea-surface elevation between the two ocean basins. Today, the ITF transports relatively cool, fresh northern Pacific surface water into the Indian Ocean (Gordon and Fine, 1996; Cane and Molnar, 2001; Sengupta et al., 2013) through

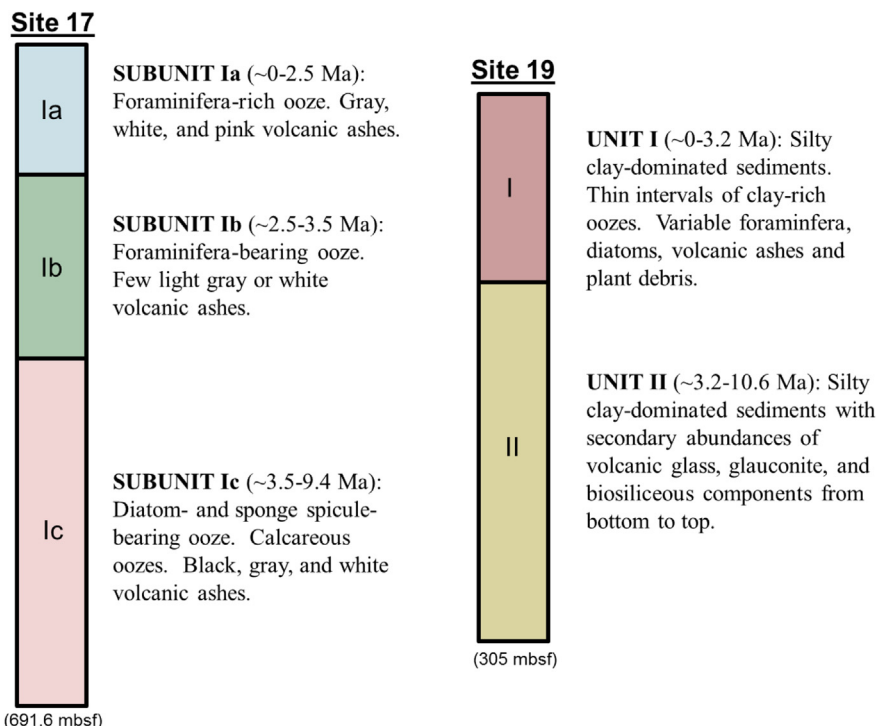


Figure 2. Generalized core stratigraphy at Sites 17 and 19 (Collett et al., 2008).

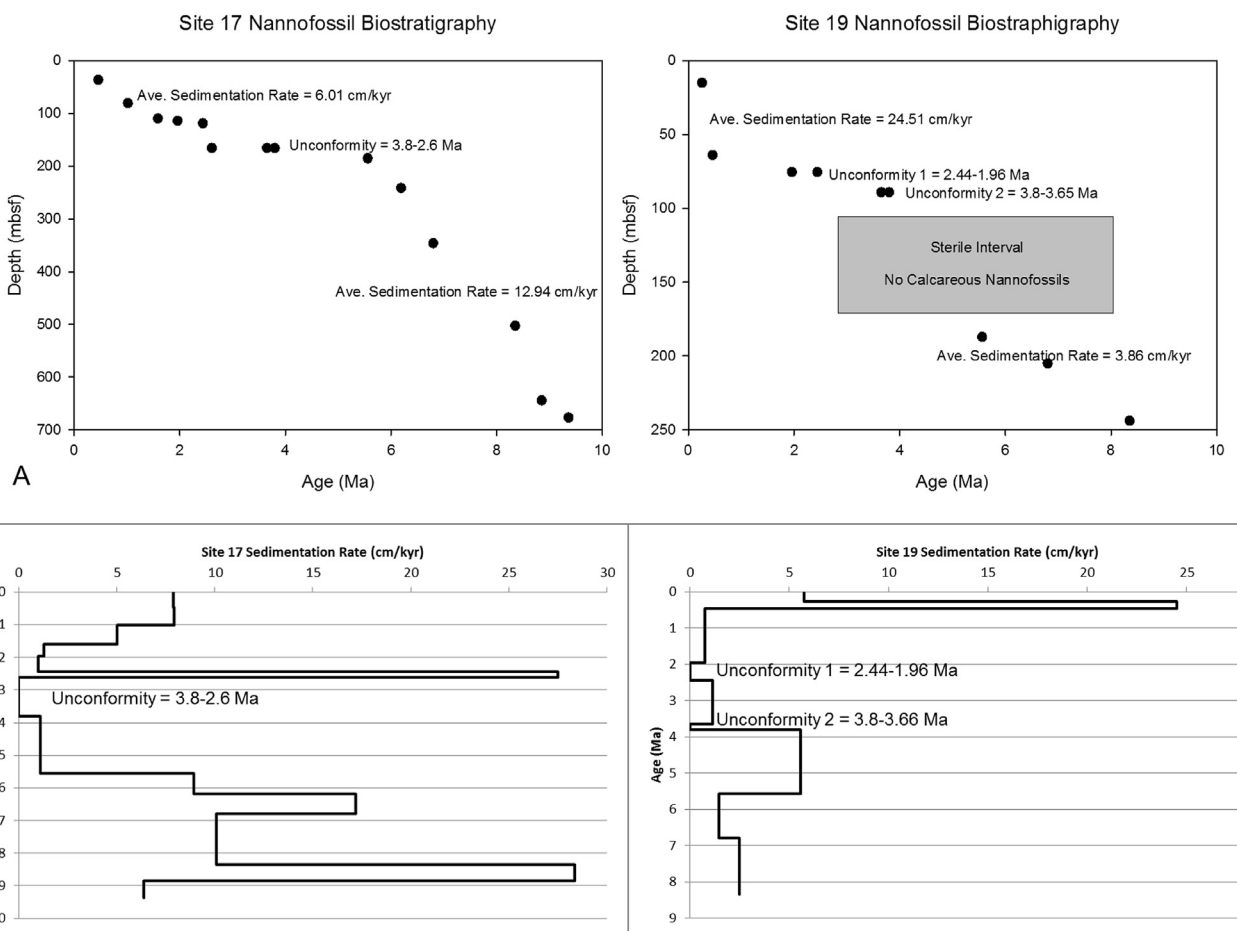


Figure 3. A) Age models (see Flores et al., 2014) at NGHP-01 Sites 17 and 19, showing the age and occurrence of unconformities within these records and the average sedimentation rates above and below the unconformities. B) Sedimentation rates at Sites 17 and 19 between discrete age control points.

numerous channels located between islands of the Indonesian archipelago and the surrounding marginal seaways, such as the South China Sea (Gordon et al., 1996, 2012; Fang et al., 2005, 2009; Tozuka et al., 2007). However, because of the narrow nature of the passageways that connect these two oceans and active tectonism throughout the region, uplift and/or subsidence of the seafloor (Nishimura and Suparka, 1997; Martin and Scher, 2006; Rai and Singh, 2012), as well as eustatic sea-level falls during the mid-late Miocene and present (Haq et al., 1987) may have periodically restricted deep water mass flow between these basins or re-routed flow paths (e.g., Gordon and Fine, 1996; Fang et al., 2010; Susanto et al., 2010, 2012), potentially limiting the exchange of nutrients between the western Pacific and eastern Indian Oceans (Gourlan et al., 2007; Jiang et al., 2007). Geotectonic (e.g., Nishimura and Suparka, 1997), paleontological (e.g., Kennett et al., 1985), and geochemical (e.g., Martin and Scher, 2006) datasets from the southern Indian and western Pacific Oceans have revealed the progressive restriction of the ITF from early to late Miocene (~23.7 Ma–5.3 Ma). Deep water flow through the ITF is believed to have been more or less closed and/or re-routed by ~6 Ma (Kennett et al., 1985; Hall, 1996, 2002; Nishimura and Suparka, 1997). More recent studies show that deep water mass exchange through the ITF was periodically re-established after ~6 Ma, with complete closure or re-routing of the deep waters being more recent, around ~4–3 Ma (late Pliocene) (e.g., Cane and Molnar, 2001; Gourlan et al., 2007).

The World Ocean Atlas 09 indicates that the modern distribution of dissolved nutrients for the Pacific Ocean is higher than that of the Indian ocean (Garcia et al., 2010). More specifically, the Pacific Ocean contains higher concentrations of silicate, phosphate, and nitrate with depth as well as for surface water masses (Buranapratheprat et al., 2010; Garcia et al., 2010). Concentrations of these nutrients are highest in the northern Pacific Ocean, where ITF waters originate in the modern ocean (Cane and Molnar, 2001). Prior to ~4–3 Ma, the source of ITF waters was from the warm, comparatively less nutrient-rich South Pacific (Cane and Molnar, 2001).

5. Methods

The mass accumulation of biogenic silica (BSi) in marine sediments is a function of the surface water plankton productivity in the ocean and often correlates with the flux of marine organic carbon and calcium carbonate (from plankton) to the seafloor (e.g., Calvert, 1966; Lyle et al., 1988). Shipboard smear-slide and coarse-fraction analyses of the sediments at Sites 17 and 19 revealed a decrease in the relative abundance of biosiliceous marine organisms from the base to the top of the cores in both records (Collett et al., 2008) and it is this change that is the focus of this study. Preservation of biosiliceous sediments within these records is good throughout the timeframe studied based on the quality of silica tests examined in smear slides (Collett et al., 2008). Bulk sediment samples from NGHP-01 Sites 17 and 19 were initially dried and then powdered using a mortar and pestle. Powdered samples were placed in individually labeled sample vials and stored in a desiccator until biogenic silica analyses were made. These same samples were also analyzed for CHN elemental abundance as well as bulk Corg isotopic analysis (Johnson et al., 2014).

Biogenic silica (BSi) was determined on 68 bulk sediment samples from Site 17 and 56 samples from Site 19 by extracting BSi from ~25 mg of sample material using a modified version of the wet alkaline technique of DeMaster (1981) and Strickland and Parsons (1972), which are outlined in the Stanford University Stable Isotope Laboratory Standard Operating Procedure Manual (Mucciarone, 2003). This procedure uses a 0.1 M NaOH solution at a

constant temperature of 85 °C to leach silica from the sample (Mucciarone, 2003). Sequential sampling of each sample was performed at 30 min and at each hour from hours 1–5 in order to establish a robust BSi leaching curve. After the allotted sampling interval was complete, a molybdate reagent and a reducing solution were added to turn each sample a hue of blue that corresponds to the concentration of silica (deeper blue for greater silica content). Standards were prepared to cover the range of sample concentrations. Standards and samples were then analyzed on a Milton Roy Spectronic 501/601 spectrophotometer at a wavelength of 812 nm. Absorbance at this wavelength varies from 3.000 to 0.000 with analytical precision of ± 0.001 . The absorbance value of each sample was measured 3–4 times, or until two consecutive readings indicated the absorbance of the sample had stabilized. The average of these two analyses was then plotted relative to the aliquot sampling interval (time). Each individual sample thus has a corresponding plot containing six absorbance analyses, one at 30 min and five for each of the successive hours (1–5) plotted relative to time (Fig. 4). In order to determine the total weight percent BSi, a least-squares regression analysis was performed on the increase in BSi extracted versus time. Early extractions (hours ~0–2) target the dissolution of amorphous silica (BSi or volcanic glass), whereas later ones target Si from minerals (i.e., clay, feldspars, quartz). It is noteworthy that all of the samples analyzed for BSi in this study were from non-volcanic ash bearing intervals in both the Site 17 and Site 19 records. Therefore, the y-intercept of the extrapolated best-fit trendline from the least-squares regression is representative of the biogenic silica concentration for an individual sample (Fig. 4). The best-fit linear regressions for all samples equaled or exceeded $R^2 = 0.9$ (Fig. 4). In order to convert the BSi absorbance for each sample to a concentration, these values were compared to the standard curve of absorbance versus concentration. The following silica standard concentrations were prepared by diluting a 1000 ppm SiO₂ (~35,606.2 μM Si) standard solution (Ricca Chemical) with Milli-Q water (18.2 MΩ * cm at 25 °C): 0 μM Si; 125 μM Si; 463 μM Si; 908 μM Si; 1193 μM Si. The standard curve of absorption ($R^2 > 0.999$) was run at the start and end of each sampling session to account for potential instrument drift. High (1193 μM Si) and low (125 μM Si) standards, and a sample of Milli-Q water were also analyzed after each time-specific (i.e., 30 min, 1 h, 2 h, etc.) suite of

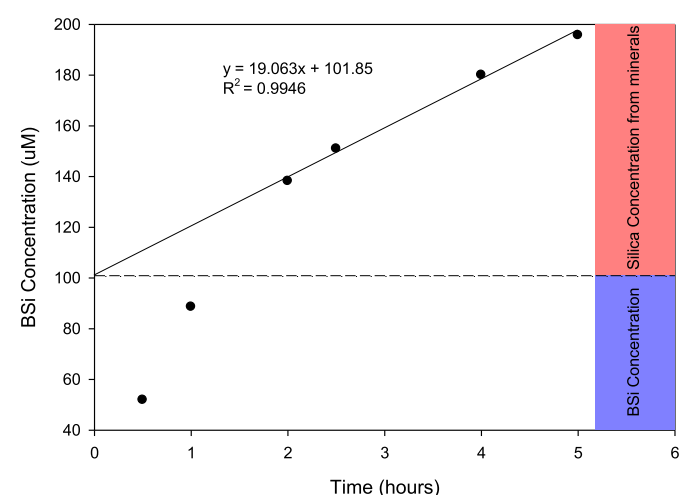


Figure 4. Time-integrated silica dissolution example for a sample from the northeast Indian Ocean. The first two points target biologic SiO₂. The last four points represent the slower dissolution of mineral SiO₂. The slope-break in the data occurs because of the different dissolution rates of amorphous and mineral SiO₂ components. The y-intercept of the linear regression through the last four data points is the concentration of BSi in this sample.

Table 1
Biogenic silica MAR at NGHP-01 sites 17 and 19.

Site	17	17	17	17	17	17	17	17	17	17	17	17	17	17
Sample	1H2 40-42	2H4 40-42	3H7 40-42	5H2 38-40	6H3 40-42	7H7 40-42	8H7 40-42	10H6 40-42	12H1 38-40	13X2 40-42	14X3 40-42	16X2 40-42	16X6 40-42	
Depth (mbsf)	2.40	9.40	22.90	34.88	45.84	61.40	70.40	88.40	99.88	110.90	121.90	139.60	145.29	
BSi (wt %)	0.20	0.15	0.16	0.15	0.22	0.16	0.18	0.19	0.26	0.14	0.19	0.21	0.19	
Age (Ma)	0.03	0.12	0.29	0.44	0.58	0.78	0.89	1.17	1.40	1.70	2.45	2.52	2.54	
BSi MAR (g/cm ² * kyr)	0.01	0.01	0.01	0.01	0.02	0.01	0.01	0.01	0.01	0.00	0.06	0.06	0.06	
Site	17	17	17	17	17	17	17	17	17	17	17	17	17	17
Sample	18X2 41-43	18X4 41-43	18X5 41-43	19X2 40-42	19X4 41-43	19X6 40-42	21X2 40-42	22X1 38-40	22X6 40-42	24X4 13-15	25X5 40-42	27X1 42-44	28X1 40-42	
Depth (mbsf)	157.97	160.97	162.47	166.73	169.73	172.73	178.40	185.58	192.79	206.68	219.50	233.22	242.90	
BSi (wt %)	0.15	0.23	0.24	0.26	0.21	0.21	0.19	0.19	0.16	0.21	0.44	0.59	0.65	
Age (Ma)	2.58	2.59	2.60	3.90	4.17	4.44	4.95	5.56	5.64	5.80	5.94	6.10	6.20	
BSi MAR (g/cm ² * kyr)	0.05	0.07	0.07	0.00	0.00	0.00	0.02	0.02	0.02	0.04	0.06	0.13		
Site	17	17	17	17	17	17	17	17	17	17	17	17	17	17
Sample	29X3 41-43	30X3 40-42	31X2 40-42	32X5 40-42	33X2 39-41	34X1 38-40	34X4 40-42	35X1 41-43	36X4 40-42	39X4 40-42	40X6 38-40	41X6 50-52	42X4 40-42	
Depth (mbsf)	254.45	264.00	271.38	285.67	291.25	299.58	304.10	309.21	322.24	334.90	344.06	354.57	361.19	
BSi (wt %)	0.49	0.58	0.51	0.76	0.84	0.86	0.84	1.04	1.69	1.62	1.36	1.53	1.87	
Age (Ma)	6.26	6.32	6.36	6.45	6.48	6.53	6.55	6.58	6.66	6.73	6.79	6.88	6.95	
BSi MAR (g/cm ² * kyr)	0.10	0.11	0.10	0.15	0.16	0.17	0.16	0.20	0.33	0.32	0.26	0.15	0.18	
Site	17	17	17	17	17	17	17	17	17	17	17	17	17	17
Sample	43X6 9-11	45X1 40-42	46X1 40-42	47X3 10-12	47X7 38-40	51X1 42-44	52X2 41-43	53X5 40-42	54X5 40-42	55X8 40-42	56X2 40-42	58X4 32-34	61X5 37-39	
Depth (mbsf)	372.12	386.10	395.80	407.70	413.21	424.72	435.91	448.58	458.64	469.52	474.10	496.10	506.85	
BSi (wt %)	2.03	1.47	1.42	2.15	1.57	1.71	2.30	1.65	2.49	1.76	2.00	2.46	2.40	
Age (Ma)	7.05	7.19	7.29	7.41	7.46	7.58	7.69	7.81	7.91	8.02	8.07	8.29	8.36	
BSi MAR (g/cm ² * kyr)	0.19	0.14	0.13	0.20	0.15	0.16	0.22	0.16	0.24	0.17	0.19	0.23	0.63	
Site	17	17	17	17	17	17	17	17	17	17	17	17	17	17
Sample	62X7 30-32	64X3 35-37	65X2 40-42	66X1 42-44	67X7 39-41	68X5 41-43	69X3 40-42	73X2 40-42	74X2 40-42	75X5 36-38	77X2 33-35	77X6 40-42	78X5 46-48	
Depth (mbsf)	519.41	533.22	541.90	550.12	565.50	573.50	582.10	598.90	608.60	622.13	635.57	640.68	649.17	
BSi (wt %)	1.88	1.75	2.53	2.10	2.13	2.15	2.32	2.20	3.28	2.80	2.67	2.31	3.12	
Age (Ma)	8.41	8.46	8.49	8.52	8.57	8.60	8.63	8.69	8.72	8.77	8.82	8.84	8.93	
BSi MAR (g/cm ² * kyr)	0.49	0.46	0.66	0.55	0.56	0.56	0.61	0.58	0.86	0.74	0.70	0.61	0.19	
Site	17	17	17	19	19	19	19	19	19	19	19	19	19	19
Sample	80X5 36-38	82X3 38-40	83X1 42-44	1H1 40-42	2H1 40-42	3H3 40-42	3H6 40-42	4H6 38-40	6H1 43-45	7H5 40-42	7H7 40-42	8H1 40-42	8H2 40-42	
Depth (mbsf)	667.28	675.38	683.32	0.40	5.70	18.20	22.70	32.18	43.73	59.20	62.20	66.70	67.38	
BSi (wt %)	2.00	2.20	3.26	0.35	0.26	0.14	0.31	0.30	0.27	0.31	0.29	0.17	0.26	
Age (Ma)	9.21	9.34	9.46	0.01	0.10	0.27	0.29	0.33	0.38	0.44	0.45	0.81	0.90	
BSi MAR (g/cm ² * kyr)	0.12	0.13	0.20	0.02	0.01	0.03	0.07	0.07	0.06	0.07	0.07	0.00	0.00	
Site	19	19	19	19	19	19	19	19	19	19	19	19	19	19
Sample	8H4 40-42	8H5 40-42	8H7 42-44	8H8 33-35	9H1 40-42	9H2 40-42	10H2 40-42	11H1 94-96	11H3 41-43	12X3 40-42	13X3 40-42	14X3 39-41	18X2 40-42	
Depth (mbsf)	69.70	71.20	74.22	75.13	76.20	77.70	87.20	95.74	97.82	100.73	110.05	120.79	130.90	
BSi (wt %)	0.26	0.30	0.21	0.24	0.24	0.24	0.25	0.23	0.16	0.29	1.22	1.24	1.03	

Age (Ma)	1.21	1.40	1.80	1.92	2.51	2.64	3.47	3.92	3.96	4.01	4.17	4.37	4.55
BSi MAR (g/cm ² * kyr)	0.00	0.00	0.00	0.00	0.00	0.00	0.00	0.01	0.01	0.01	0.06	0.06	0.05
Site	19	19	19	19	19	19	19	19	19	19	19	19	19
Sample	18X6 40-42	20X4 40-42	21X5 40-42	22X4 40-42	23X3 43-45	24X1 40-42	24X4 40-42	24X6 40-42	28X2 40-42	28X7 40-42	28X7 40-42	29X2 40-42	29X5 40-42
Depth (mbsf)	136.88	153.20	164.29	172.40	180.53	187.20	194.70	197.13	199.83	203.22	206.82	211.32	
BSi (wt %)	0.34	0.59	0.87	0.33	0.30	0.26	0.48	0.42	0.34	0.50	0.85	0.83	
Age (Ma)	4.66	4.95	5.15	5.30	5.44	5.57	6.08	6.25	6.44	6.67	6.87	7.05	
BSi MAR (g/cm ² * kyr)	0.02	0.03	0.04	0.02	0.02	0.00	0.00	0.01	0.01	0.01	0.02	0.02	0.02
Site	19	19	19	19	19	19	19	19	19	19	19	19	19
Sample	30X2 40-42	30X5 40-42	31X2 40-42	31X5 40-42	32X2 40-42	32X5 40-42	33X1 40-42	33X3 40-42	33X5 35-37	34X1 39-41	34X2 36-38	34X4 39-41	35X6 40-42
Depth (mbsf)	216.15	219.55	226.81	231.31	236.05	240.54	244.80	249.72	254.39	254.93	257.96	270.86	
BSi (wt %)	1.68	1.24	1.20	1.40	1.59	2.02	0.87	1.59	0.49	1.30	1.15	1.30	
Age (Ma)	7.24	7.38	7.67	7.85	8.04	8.22	8.39	8.46	8.58	8.77	8.79	9.43	
BSi MAR (g/cm ² * kyr)	0.04	0.03	0.03	0.03	0.04	0.05	0.02	0.04	0.01	0.03	0.03	0.03	
Site	19	19	19	19	19	19	19	19	19	19	19	19	19
Sample	36X1 40-42	36X2 39-41	36X4 42-44	36X6 37-39	36X6 37-39	36X6 37-39	37X4 40-42	37X4 40-42	38X1 40-42	38X1 40-42	38X5 40-42	38X5 40-42	
Depth (mbsf)	273.70	275.19	277.97	280.66	286.98	292.80	292.80	292.80	292.80	292.80	292.80	292.80	
BSi (wt %)	1.48	1.64	1.16	1.40	1.12	0.76	0.76	0.76	0.76	0.76	0.48	0.48	
Age (Ma)	9.54	9.60	9.71	9.82	10.07	10.30	10.30	10.30	10.30	10.30	10.54	10.54	
BSi MAR (g/cm ² * kyr)	0.04	0.04	0.03	0.03	0.03	0.03	0.03	0.03	0.03	0.03	0.02	0.02	

samples was analyzed in order to evaluate instrument drift and/or inaccuracies.

Biogenic silica weight percentage was determined on bulk samples from Sites 17 and 19 at fairly regularly spaced intervals throughout the cores. Weight percent BSi for each measured sample was later converted into an instantaneous mass accumulation rate for discrete sampling intervals throughout the cores. Mass accumulation rates were calculated by multiplying the linear sedimentation rate (LSR) from the calcareous nannofossil age model (Fig. 3) by the dry bulk density (DBD), determined from physical properties measurements (Collett et al., 2008), and the weight percent BSi.

6. Results

The cores at Sites 17 and 19 were sampled at relatively constant ~100–300 kyr intervals from the top of each core to the base. The relatively coarse resolution of the sampling intervals permits the discussion of only general trends in the data at both core locations over million year time scales (Table 1).

The results from Site 17 are divided into three discrete intervals: 1) a section of relatively high BSi accumulation from ~9.46 Ma to ~5 Ma; 2) two segments of relatively low biogenic silica accumulation, one from ~5 Ma to ~4 Ma and another from ~1.7 Ma to the present; and 3) a period of increased BSi accumulation that occurred ~2.5 Ma (Fig. 5). The first interval exhibits variable rates of BSi accumulation that range between ~0.7 g/cm² * kyr at ~8.5 Ma and ~0.002 g/cm² * kyr at ~5 Ma. BSi initially increased within this interval from ~0.12 g/cm² * kyr at ~9.2 Ma to the highest measured value of ~0.7 g/cm² * kyr at ~8.5 Ma. Mass accumulation rates subsequently decreased from ~8.2 Ma and reached values of ~0.14 g/cm² * kyr by ~7.2 Ma before they increased again to ~0.3 g/cm² * kyr by ~6.7 Ma. Despite this variability, the mass accumulation rates of BSi throughout this interval are the highest recorded MARs in the core. The second highest observed mass accumulation rate of BSi at Site 17 occurred from ~2.6 Ma to ~1.7 Ma with rates that attained a peak of ~0.07 g/cm² * kyr at ~2.5 Ma. This pulse in BSi accumulation, however, is truncated between ~3.8 Ma–2.6 Ma because of a hiatus (most likely an unconformity) in the nannofossil biostratigraphy (Flores et al., 2014). It is therefore difficult to say exactly when the relative increase in BSi accumulation began, following the period of low BSi accumulation between ~5 Ma and ~4 Ma, but the overall trend is that of gradual increase in BSi MAR between ~5 and 4 Ma (Fig. 5). The accumulation of BSi has remained low in the Andaman Sea region at Site 17 since ~1.7 Ma. In general, the MAR of biogenic silica at Site 17 decreased from ~9.4 Ma to ~5 Ma and never returned to the pre-crash BSi levels observed during the late Miocene.

The data from Site 19 are somewhat more variable than those from Site 17 and the BSi MAR is an order of magnitude lower overall at Site 19 (Figs. 4 and 5, Table 1). The record of biogenic silica accumulation at Site 19 is divided into four discrete intervals: 1) a section of moderately high BSi accumulation that ranged between ~0.01 g/cm² * kyr at ~10.5 Ma and ~0.006 g/cm² * kyr at ~6.3 Ma with a maximum rate of accumulation of ~0.05 g/cm² * kyr at ~8.22 Ma; 2) a second period of moderately high BSi accumulation that ranged between ~0.004 g/cm² * kyr at ~5.5 Ma and ~0.003 g/cm² * kyr at ~3.8 Ma with a maximum rate of accumulation of ~0.06 g/cm² * kyr at ~4.2 Ma; 3) a third section of maximum BSi accumulation that ranged between ~0.001 g/cm² * kyr at ~0.8 Ma and ~0.02 g/cm² * kyr at present and consists of the highest rates of accumulation of ~0.07 g/cm² * kyr at ~0.4 Ma; 4) three periods of low BSi accumulation: one between ~6.3 Ma and ~5.5 Ma, a second between ~3.65 Ma and 2.44 Ma, and a third from ~1.96 to 0.8 Ma (Fig. 5). A hiatus (most likely an unconformity) in the nannofossil

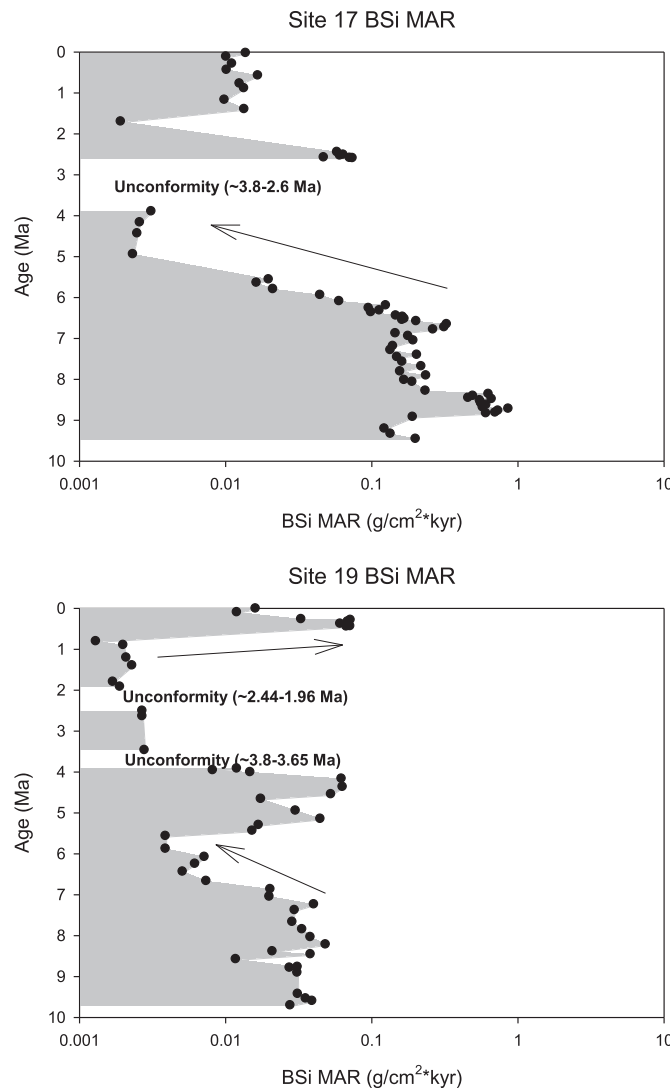


Figure 5. Biogenic silica mass accumulation rates at Sites 17 and 19 with respect to age in the core. BSi MAR is higher at Site 17 in the Andaman Sea compared to Site 19 in the Mahanadi Basin.

biostratigraphy from ~3.8 to 3.65 Ma and ~2.44–1.96 Ma prohibit interpretations within these intervals (Flores et al., 2014). In general, the MAR of biogenic silica at Site 19 decreased from ~10.5 Ma to ~5.5 Ma, with productivity recovering more rapidly following the BSi crash at ~6 Ma compared to Site 17. We consider the dramatic decrease in BSi MAR at Site 17 from ~9.4 to 5 Ma and at Site 19 from ~10.5 to 5.5 Ma to be time-coincident in the Andaman Sea and Bay of Bengal, and correlative to the reduction of BSi MAR reported in the South China Sea (Wang et al., 2004), California margin (Farrell et al., 1995; Janecek, 2000), and elsewhere in the Pacific (Cortese et al., 2004) and Indian Oceans (Dickens and Owen, 1999).

7. Discussion

Quantitative analysis of percent biogenic silica has been the focus of few studies in the Indian Ocean (Bohrmann and Ehrmann, 1991; Hempel and Bohrmann, 1990; Schmitz, 1987). These studies provide evidence of two distinct phases of biogenic opal productivity in the Indian Ocean, one from the Eocene-Oligocene (~35.8 Ma) and a second from late middle to late Miocene (~11 Ma) (Baldauf et al., 1992). To date, however, no studies of BSi

exist that have focused on long timescale productivity changes in the northern Bay of Bengal or Andaman Sea regions.

The use of biogenic silica as a proxy for productivity in the water column can be difficult to interpret, particularly in regions where volcanic glass is pervasive. Fortunately, the time-integrated dissolution steps used in the modified wet alkaline technique of DeMaster (1981) and Strickland and Parsons (1972) accounts for the different rates of dissolution of amorphous and mineral phases and therefore facilitates the identification of impure volcanic glass versus BSi signatures. Moreover, the discretionary selection of samples from intervals within the core devoid of volcanic ashes acts as a first step in ensuring the analysis for BSi does not contain a significant signature from volcanic glasses. The purity of BSi signatures from Site 17 is not only revealed from the slope breaks in the time-integrated dissolution datasets (Fig. 4), but also in a plot of the downhole porewater Si concentration (Fig. 6). The concentration of silica in pore fluids from Site 17 varies such that the core may be divided into three intervals: 1) an interval of high porewater Si from ~9.5 Ma–5.7 Ma, 2) a section of low porewater Si from ~5.7 Ma–2.6 Ma, and 3) an interval of moderately high porewater Si concentration from ~2.6 Ma–0.5 Ma. In the record at Site 17, the porewater Si concentration (Fig. 6) is highest in the core near the bottom (~9.5–5.7 Ma), where the mass accumulation rate of BSi is high and there are also abundant volcanic ashes. In the middle of the core (~5.7–2.6 Ma), where no continuous volcanic ash layers are present, although disseminated ashes are observed in low abundances and the BSi MAR is low, the porewater Si concentrations are low. In contrast to both of the deeper portions of the core, the top of the core (the last ~2.6 Myrs) shows a bulge in porewater Si that corresponds with the occurrence of volcanic glass, and a nearly constant and low occurrence of BSi (Fig. 6). These results imply that the sediment porewater silica at Site 17 may be largely derived from dissolution of volcanic glass phases. If the measurements of BSi in the uppermost part of the record at Site 17

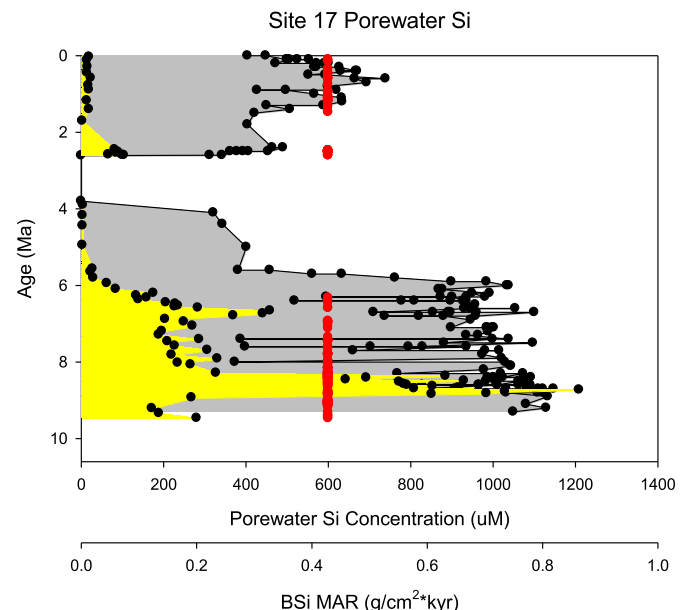


Figure 6. Porewater Si concentrations (gray area fill) and BSi MAR (yellow area fill) at Site 17 with respect to age within the core and ages of known occurrences of volcanic ashes (red dots). Porewater Si concentrations (Rose et al., 2014) appear to be primarily derived from amorphous volcanic glass phases, particularly in Subunits Ia and Ib, rather than the dissolution of biogenic silica tests, as evidenced by the covariance of ashes and high porewater [Si]. (For interpretation of the references to color in this figure legend, the reader is referred to the web version of this article.)

(~2.6–0 Ma) had incorporated volcanic glass, the BSi profile would more closely match the porewater profile in this interval. Instead, the porewater profile covaries with the abundance of volcanic glass in the record, particularly in Subunits Ia and Ib, where biogenic silica is less abundant. Porewater Si in Subunit Ic is most likely comprised of an admixture of both BSi and amorphous silica from volcanogenic sources. Coupled with the strength of separation in the slope-breaks from the time-integrated BSi dissolutions (Fig. 4), the BSi data reported here do not include a significant signature from volcanic glass in the Site 17 record. Because Site 19 is located farther from the Sunda volcanic arc and only one ash occurrence was documented in the core (Collett et al., 2008), the BSi measurements here are not affected by amorphous volcanic glasses.

The sedimentary records from Sites 17 and 19 are distinct from one another as a result of their different depositional settings. Site 17 preserves a predominantly marine pelagic record that contains variable amounts of airfall volcanic ashes and fine grained (clay-sized) clastic materials (Collett et al., 2008). In contrast, Site 19 is predominantly a hemipelagic record that consists of variable concentrations of marine carbonate and biosiliceous fossils, terrestrial plant remains, and clastic detritus that most likely originated from the Mahanadi River (Collett et al., 2008; Phillips et al., 2014). Despite these differences, shipboard smear-slide and coarse-fraction analyses of these records revealed a general pattern of decreased biosiliceous fossils from the bottom to the top of the cores. These observations are now quantified through wet chemical analytical techniques and reveal the timing of a significant crash in the BSi MAR at both Sites 17 and 19. In general, the biogenic silica crash at Site 17 occurred between ~6.7 and 5 Ma, whereas the crash at Site 19 occurred between ~7.2 and 5.5 Ma. The crash in both core locations is time-correlative. The duration of low BSi MAR that followed the crash at Site 17 is difficult to estimate due to the presence of an unconformity that lasted from ~3.8 to 2.6 Ma, but a moderate pulse in productivity is apparent that began prior to ~3.8 Ma and continued after ~2.6 Ma. In contrast, BSi MAR rebounded at Site 19 after a period of low productivity that lasted approximately 0.7 Myr. Despite the different environments of deposition between these two core locations, biogenic silica productivity noticeably decreased between ~7.2 and 5 Ma at both core locations. This crash is correlative to the reduction of BSi reported in the South China Sea (Wang et al., 2004), California margin (Farrell et al., 1995; Janecek, 2004), and elsewhere in the Pacific (Cortese et al., 2004) and Indian Oceans (Dickens and Owen, 1999).

Numerous studies (e.g., Kennett et al., 1985; Martin and Scher, 2006; Nishimura and Suparka, 1997) of the southern Indian Ocean and western Pacific Ocean have correlated changes in geotectonic, paleontological and geochemical datasets to the progressive restriction of the Indonesian Throughflow (ITF) over long timescales. The timescale (~23.7 Ma–5.3 Ma) of these changes makes it difficult to rectify orbital to sub-orbital scale changes, but may reflect longer timescale changes in sedimentation rates and ocean productivity due to large changes in the Indian monsoon system or oceanographic change. These datasets suggest that the flow of deep, nutrient-rich Pacific Ocean waters through the ITF became restricted by ~6 Ma (Hall, 1996, 2002; Kennett et al., 1985; Nishimura and Suparka, 1997; Martin and Scher, 2006), but was perhaps periodically re-established thereafter to give rise to more recent (late Pliocene ~4–3 Ma) estimates of complete deep water restriction (e.g., Cane and Molnar, 2001; Gourlan et al., 2007). The timing of the primary biogenic silica crash at Sites 17 and 19 (~7.2–5 Ma) in the Andaman Sea and northern Bay of Bengal, as well as opal MARs from ODP Site 1143 in the South China Sea (Wang et al., 2004) provide evidence of a dramatic change in paleo-productivity coincident in time with estimates for the timing of the restriction of the ITF at ~6 Ma.

Upwelling-induced productivity for the last ~40 kyr in the Bay of Bengal and Arabian Sea has been related to variations in the strength of the summer monsoon (e.g., Schubert et al., 1998; Sijinkumar et al., 2010). When the summer monsoon is strong, increased rainfall over the Indian subcontinent provides a high supply of H_4SiO_4 -rich runoff to the Indian offshore region and enhanced southwesterly-directed winds that could potentially promote upwelling (Filippelli, 1997; Dettman et al., 2001; Gregg, 2002; Gupta and Thomas, 2003; Hathorne and James, 2006; Clift et al., 2008). Upwelling-induced productivity, however, has been shown to be severely limited due to freshwater runoff during the summer monsoon, particularly along the continental shelf and slope, where a wedge of low salinity, low nutrient surface water stratifies the water column and inhibits productivity (Prassana Kumar et al., 2002; Madhupratap et al., 2003; Bolton et al., 2013). Over the past 110 kyr, biological productivity at Site 19 decreased during periods of enhanced summer monsoon intensity; however, BSi MAR increased relative to $CaCO_3$ MAR during these periods of intensified summer monsoon (Phillips et al., 2014), suggesting BSi MAR may be decoupled from overall productivity and related to silicate availability in the northern Bay of Bengal. In the semi-restricted Andaman Sea, upwelling-induced productivity occurs as a result of mesoscale cyclonic eddies generated due to seasonal fluctuations in the monsoonal winds (Wyrtki, 1961; Buranapratheprat et al., 2010; Rizal et al., 2012). On million year timescales, BSi MAR data from both Sites 17 and 19 record the same decrease in BSi MAR from ~7.2 to 5 Ma. Differences in BSi MAR since ~5 Ma between the two sites are most likely attributed to the proximity of point sources of nutrients such as the Mahanadi, Irrawaddy, and Ganges–Brahmaputra Rivers or localized sites of upwelling that may have provided a means of sustaining the most recent pulses in BSi productivity at Sites 17 and 19, particularly during phases of reduced monsoon intensity.

The abrupt decrease in productivity of biogenic silica at Sites 17 and 19 from ~7.2 to 5 Ma is consistent with geochemical, paleontological, and geotectonic datasets that support the gradual restriction of the gateway linking deep Pacific Ocean water masses to the Indian Ocean via the Indonesian Throughway from early to late Miocene (~23.7 Ma–5.3 Ma). Today, the Andaman Sea region has limited deep water hydrographic communication to the South China and Java Seas through the Strait of Malacca (Keller and Richards, 1967; Rizal et al., 2012). However, the flow into and out of this region may have been enhanced prior to ~6 Ma and could have provided enough vital nutrients to the Site 17 region and even into the Bay of Bengal to sustain high rates of BSi surface productivity in both regions. As communication between the Andaman Sea and the ITF gradually decreased, the mass accumulation rates of BSi also decreased. By ~6.7–5 Ma, the influx of nutrients that sustained BSi productivity may have been limited resulting in the observed crash in the BSi MAR. A short pulse in BSi productivity at Site 17 between ~4 and 2.5 Ma could reflect riverine sources of nutrients from the nearby Irrawaddy and Ganges–Brahmaputra Rivers and/or favorable localized upwelling. The pattern of BSi MAR at Site 17 are nearly identical to those observed at ODP Site 1143 in the South China Sea (Wang et al., 2004) and supports previous studies that report diminished ITF transport by ~6 Ma (e.g., Hall, 1996, 2002; Kennett et al., 1985; Nishimura and Suparka, 1997; Martin and Scher, 2006). Because this time interval spans the unconformity from ~3.8 to 2.6 Ma at Site 17, however, it is difficult to assess the true signature of any recovery of BSi in the Andaman Sea. The cessation of this secondary pulse in BSi productivity at Site 17 is consistent with a late Pliocene (~4–3 Ma) estimate for the final restriction of deep water mass flow through the ITF from Cane and Molnar (2001) and Gourlan et al. (2007). Alternatively, enhanced supply of nutrient-rich freshwater from the nearby Irrawaddy and

Mahanadi Rivers in response to the documented increase in the intensity of the Indian monsoon at ~5 Ma (Zhisheng et al., 2001; Curray et al., 2003; Gupta and Thomas, 2003) may have initiated the increase in productivity after this time.

Tracking the flow of Pacific Ocean water masses as they flow through the ITF and into the Indian Ocean has been the focus of numerous studies (e.g., Lee et al., 2002; Valsala and Ikdea, 2007; Sengupta et al., 2013). In general, once entering the Indian Ocean, ITF waters flow westward across the Indian Ocean and upon reaching the western boundary, re-route into three branches: 1) an eastward-flowing branch located just south of the equator, 2) an eastward-flowing branch located just north of the equator, 3) a northward-flowing branch that ultimately upwells in the Somali region and spreads as surface waters across the northern Indian Ocean (Valsala and Ikdea, 2007). The third branch of the ITF within the Indian Ocean may have had a profound effect on surface-water productivity in the Site 19 region. In particular, the restriction of and concomitant re-routing of ITF waters around Australia at ~6 Ma may explain the similar timing of the BSi MAR crash at Site 19 (~7.2–6.3 Ma) to the BSi MAR crash that occurred in the Andaman Sea and elsewhere in the southern Indian and Pacific Oceans, as well as marginal seaways such as the South China Sea. Because the ITF is much more modulated in the vastly larger Indian Ocean compared to the semi-restricted Andaman Sea, the effects of a reduction in ITF may have been less pronounced in the northern Indian Ocean. Nevertheless, the crash in BSi MAR at Sites 17 and 19 is coincident and most likely reflects a major change in the delivery of nutrient-rich deep Pacific Ocean waters to the Bay of Bengal and Andaman Sea. The relatively rapid recovery of BSi MAR at Site 19 was likely primarily controlled by surface-water runoff and regionally derived nutrients from the Indian subcontinent (e.g., Farrell et al., 1995; Filippelli, 1997; Dettman et al., 2001; Gupta and Thomas, 2003; Hathorne and James, 2006; Clift et al., 2008), which would have increased with the documented strengthening of the monsoon after ~5 Ma (Zhisheng et al., 2001; Curray et al., 2003; Gupta and Thomas, 2003).

8. Conclusions

Quantitative analysis of biogenic silica was performed on 68 bulk sediment samples from NGHP-01 Site 17 and 56 samples from NGHP-01 Site 19 in order to better understand an abrupt crash in biogenic silica at both of these sites. The primary BSi crash at both of these northeast Indian Ocean sites occurred between ~7.2 and 5 Ma, which is in good agreement with previously reported studies of the geotectonics, paleontological and geochemistry of marine sediments from the southern Indian Ocean and western Pacific Ocean, which document the closure of the Indonesian Throughflow at ~6 Ma. In contrast to BSi mass accumulation rates observed in sediments from the northern Bay of Bengal at Site 19, which appear to be influenced heavily by freshwater runoff that emanated from the Mahanadi River, those of the Andaman Sea region appear to have been much more sensitive to changes in the ITF. Biogenic silica within the Andaman Sea region never fully recovered to late Miocene levels following the closure of a northern lobe of ITF between ~6.7 and 5 Ma, whereas productivity at Site 19 was rejuvenated coincident with the proposed strengthening of the monsoon after ~5 Ma.

Acknowledgments

The authors wish to thank those that contributed to the success of the National Gas Hydrate Program Expedition 01 (NGHP-01). NGHP-01 was planned and managed through collaboration between the Directorate General of Hydrocarbons (DGH) under the

Ministry of Petroleum and Natural Gas (India), the U.S. Geological Survey (Contract # 07CRSA0708) (USGS), and the Consortium for Scientific Methane Hydrate Investigations (CSMHI) led by Overseas Drilling Limited (ODL) and FUGRO McClelland Marine Geosciences. The platform for the drilling operation was the research drill ship *JOIDES Resolution*, operated by ODL. Much of the drilling/coring equipment used was provided by the Integrated Ocean Drilling Program (IODP) through a loan agreement with the US National Science Foundation. The financial support for NGHP-01, from the Oil Industry Development Board, Oil and Natural Gas Corporation Ltd., GAIL (India) Ltd., and the Oil India Ltd., is gratefully acknowledged. This research was supported by the National Gas Hydrates Program of India, the Ed Picou Fellowship Grant for Graduate Studies in Earth Sciences from the Gulf Coast Section of the Society for Sedimentary Geology, a University of New Hampshire Department of Earth Sciences Research Award and Natural Resources and Earth Systems Science Program Research Award. We thank the entire NGHP-01 Expedition shipboard science party and crew for the characterization of the stratigraphy and for the collection of the cores in 2006. The BSi measurements at UNH would not have been possible without the support of Linda Kalnejais and the generosity of Laurie Westover at the University of New Hampshire.

References

- Amiruddin, A.M., Ibrahim, Z.Z., Ismail, S.A., 2011. Water mass characteristics in the Strait of Malacca using ocean data view. *Res. J. Environ. Sci.* 5, 49–58.
- Babu, C.P., Pattan, J.N., Dutta, K., Basavaiah, N., Ravi Prasad, G.V., Ray, D.K., Govil, P., 2010. Shift in detrital sedimentation in the eastern Bay of Bengal during the late Quaternary. *J. Earth Syst. Sci.* 119, 285–295.
- Baldauf, J.G., Barron, J.A., Ehrmann, W.U., Hempel, P., Murray, D., 1992. Biosiliceous sedimentation patterns for the Indian Ocean during the last 45 million years. *American Geophysical Union, Geophys. Monogr.* 70, 335–349.
- Bastia, R., Das, S., Radhakrishna, M., 2010. Pre- and post-collisional depositional history in the upper and middle Bengal fan and evaluation of deepwater reservoir potential along the northeast continental margin of India. *Mar. Pet. Geol.* 27, 2051–2061.
- Berger, W.H., Leckie, R.M., Janecek, T.R., Stax, R., Takayama, T., 1993. Neogene carbonate sedimentation on Ontong Java Plateau: highlights and open questions. *Proc. Ocean. Drill. Program, Sci. Results* 130, 711–744.
- Bohrmann, G., Ehrmann, W.U., 1991. Analysis of sedimentary facies using bulk mineralogic characteristics in Cretaceous to Quaternary sediments from the Kerguelan Plateau: sites 737, 738 and 744. In: Barron, J.A., Larsen, B., et al. (Eds.), *Proceedings of the Ocean Drilling Program, Scientific Results*, vol. 119. Ocean Drilling Program, College Station, TX, pp. 211–223.
- Bolton, C.T., Change, L., Clemens, S.C., Kodama, K., Ikebara, M., Medina-Elizalde, M., Paterson, G.A., Roberts, A.P., Rohling, E.J., Yamamoto, Y., Zhao, X., 2013. A 500,000 year record of Indian summer monsoon dynamics recorded by eastern equatorial Indian Ocean upper water-column structure. *Quat. Sci. Rev.* 77, 167–180.
- Bowles, F., Ruddiman, W., Jahn, W., 1978. Acoustic stratigraphy, structure, and depositional history of the Nicobar Fan, Eastern Indian Ocean. *Mar. Geol.* 26, 269–288.
- Buranapratheprat, A., Laongmanee, P., Sukramongkol, N., Prommas, R., Promjinda, S., Yanagi, T., 2010. Upwelling induced by meso-scale cyclonic eddies in the Andaman Sea. *Coast. Mar. Sci.* 34, 68–73.
- Calvert, 1966. Accumulation of diatomaceous silica in the sediment of the Gulf of California. *Geol. Soc. Am. Bull.* 77, 569–572.
- Cane, M.A., Molnar, P., 2001. Closing of the Indonesian Seaway as a precursor to east African aridification around 3–4 million years ago. *Nature* 411, 157–162.
- Clift, P.D., Hodges, K.V., Heslop, D., Hannigan, R., Van Long, H., Calves, G., 2008. Correlation of Himalayan exhumation rates and Asian monsoon intensity. *Nat. Geosci.* 1, 875–880.
- Collett, T.S., Riedel, M., Cochran, J., Boswell, R., Presley, J., Kumar, P., Sathe, A., Sethi, A., Lall, M., Sibal, V., the NGHP Expedition-01 Scientists, 2008. National Gas Hydrate Program Expedition 01 Initial Reports.
- Cortese, G., Gersonde, R., Hillenbrand, C.-D., Kuhn, G., 2004. Opal sedimentation shifts in the world ocean over the last 15 Myr. *Earth Planet. Sci. Lett.* 224, 509–527.
- Curry, J.R., Emmel, F.J., Moore, D.G., 2003. The Bengal Fan: morphology, geometry, stratigraphy, history and processes. *Mar. Pet. Geol.* 19, 1191–1223.
- DeMaster, D.J., 1981. The supply and accumulation of silica in the marine environment. *Geochim. Cosmochim. Acta* 45, 1715–1732.
- Dettman, D.L., Kohn, M.J., Quade, J., Ryerson, F.J., Ojha, T.P., Hamidullah, S., 2001. Seasonal stable isotope evidence for a strong Asian monsoon throughout the past 10.7 m.y. *Geology* 29, 31–34.

- Dickens, G.R., Owen, R.M., 1994. Late Miocene–Early Pliocene manganese redirection in the central Indian Ocean: expansion of the intermediate water oxygen minimum zone. *Paleoceanography* 9, 169–181.
- Dickens, G.R., Owen, R.M., 1996. Sediment geochemical evidence for an Early–middle Gilbert (Early pliocene) productivity peak in the North Pacific red Clay Province. *Mar. Micropaleontol.* 27, 107–120.
- Dickens, G.R., Owen, R.M., 1999. The Latest Miocene–Early pliocene biogenic bloom: a revised Indian Ocean perspective. *Mar. Geol.* 161, 75–91.
- Dutta, K., Bhushan, R., Somayajulu, B.L.K., 2007. Rapid vertical mixing rates in deep waters of the Andaman Basin. *Sci. Total Environ.* 384, 401–408.
- Fang, G., Susanto, R.D., Wirasantosa, S., Qiao, F., Supangat, A., Fan, B., Wei, Z., Sulistiyo, B., Li, S., 2010. Volume, heat, and freshwater transports from teh South China Sea to Indonesian seas in the boreal winter of 2007–2008. *J. Geophys. Res. Oceans* 115, 1–11.
- Fang, G., Wang, Y., Wei, Z., Fang, Y., Qiao, F., Hu, X., 2009. Inter-ocean circulation and heat and freshwater budgets of the South China Sea based on a numerical model. *Dyn. Atmos. Oceans* 47, 55–72.
- Fang, G., Susanto, R.D., Soesilo, I., Zheng, Q., Qiao, F., Wei, Z., 2005. Notes on the upper-layer interocean circulation of the South China Sea. *Adv. Atmos. Sci. COAA Spec. Issue* 22, 946–954.
- Farrell, J.W., Raffi, I., Janecek, T.R., Murray, D.W., Levitan, M., Dadey, K.A., Emeis, K.-C., Lyle, M., Flores, J.-A., Hovan, S., 1995. Late Neogene sedimentation patterns in the eastern equatorial Pacific Ocean. In: Pisias, N.G., Mayer, L.A., Janecek, T.R., Palmer-Julson, A., van Andel, T.H. (Eds.), *Proceedings of the Ocean Drilling Program, Scientific Results*, vol. 138. Ocean Drilling Program, College Station, TX, pp. 717–756.
- Filippelli, G.M., 1997. Intensification of the Asian monsoon and a chemical weathering event in the late Miocene–Early Pliocene: implications for late Neogene climate change. *Geology* 25, 27–30.
- Flores, J.-A., Johnson, J.E., Mejia-Molina, A.E., Alvarez, M.C., Sierra, F.J., Singh, S.D., Mahanti, S., Giosan, L., 2014. Sedimentation rates from calcareous nannofossil and planktonic foraminifera biostratigraphy in the Andaman Sea, northern Bay of Bengal, and eastern Arabian Sea. *J. Mar. Pet. Geol.*
- Garcia, H.E., Locarnini, R.A., Boyer, T.P., Antonov, J.I., Zweng, M.M., Baranova, O.K., Johnson, D.R., 2010. World ocean atlas 2009. In: Levitus, S. (Ed.), *Nutrients (Phosphate, Nitrate, Silicate)*, NOAA Atlas NESDIS 71, vol. 4. U.S. Government Printing Office, Washington, D.C., p. 398.
- Gordon, A.L., Fine, R.A., 1996. Pathways of water between the Pacific and Indian Oceans in the Indonesian Seas. *Lett. Nat.* 379, 146–149.
- Gordon, A.L., Huber, B.A., Metzger, E.J., Susanto, R.D., Hurlburt, H.E., Adi, T.R., 2012. South China Sea Throughflow impact on the Indonesian Throughflow. *Geophys. Res. Lett.* 39, 1–7.
- Gourlanc, A.T., Meynadier, L., Allegre, C.J., 2007. Tectonically driven changes in the Indian Ocean circulation over the last 25 Ma: Neodymium isotope evidence. *Earth Planet. Sci. Lett.* 267, 353–364.
- Gregg, W.W., 2002. Tracking the Sea WIFs record with a coupled physical/biogeochemical/radiative model of the global oceans. *Deep Sea Res. II* 49, 81–105.
- Gupta, A.K., Thomas, E., 2003. Initiation of Northern Hemisphere glaciation and strengthening of the northeast Indian monsoon: ocean Drilling Program Site 758, eastern equatorial Indian Ocean. *Geology* 31, 47–50.
- Hall, R., 1996. Reconstructing Cenozoic SE Asia. In: Hall, R., Blundell, D. (Eds.), *Tectonic Evolution of Southeast Asia*, Geological Society of London Special Publication, vol. 106, pp. 153–184.
- Hall, R., 2002. Cenozoic geological and plate tectonic evolution of SE Asia and the SW Pacific: computer-based reconstructions, model and animations. *J. Asian Earth Sci.* 20, 353–434.
- Haque, B.U., Hardenbol, J., Vail, P.R., 1987. Chronology of fluctuating sea levels since the Triassic. *Science* 235, 1156–1167.
- Hathorne, E.D., James, R.H., 2006. Temporal record of lithium in seawater: a tracer for silicate weathering? *Earth Planet. Sci. Lett.* 246, 393–406.
- Hempel, P., Bohrmann, G., 1990. Carbonate free sediment components and aspects of silica diagenesis at Sites 707, 709 and 711. In: Duncan, R.A., Backman, J., Peterson, L., et al. (Eds.), *Proceedings of the Ocean Drilling Program, Scientific Results*, vol. 115. Ocean Drilling Program, College Station, TX, pp. 677–698.
- Ibrahim, Z.Z., Yanagi, T., 2006. The influence of the Andaman Sea and the South China Sea on water masses in the Malacca Strait. *Mer* 43, 33–42.
- Janecek, T.R., 2000. Data report: late Neogene biogenic opal data for Leg 167 sites on the California margin. In: Lyle, M., Koizumi, I., Richter, C., Moore Jr., T.C. (Eds.), *Proceedings of the Ocean Drilling Program, Scientific Results*, vol. 167. Ocean Drilling Program, College Station, TX, pp. 213–214.
- Jiang, S., Wise, S.W., Wang, Y., 2007. Cause of the Middle/Late Miocene carbonate crash: dissolution or low productivity?. In: Teagle, D.A.H., Wilson, D.S., Acton, G.D., Vanko, D.A. (Eds.), *Proceedings of the Ocean Drilling Program, Scientific Results*, vol. 206, pp. 1–24.
- Johnson, J.E., Phillips, S.C., Torres, M.E., Pinero, E., Rose, K.K., Giosan, L., 2014. Influence of total organic carbon deposition on the inventory of gas hydrate in the Indian continental margins. *J. Mar. Pet. Geol.*
- Karig, D.E., Lawrence, M., Moore, G., Curran, J., 1980. Structural framework of the fore-arc basin, NW Sumatra. *J. Geol. Soc. Lond.* 137, 77–91.
- Kawagata, S., Hayward, B.W., Gupta, A.K., 2006. Benthic foraminiferal extinctions linked to late Pliocene–Pleistocene deep-sea circulation changes in the northern Indian Ocean (ODP Sites 722 and 758). *Mar. Micropaleontol.* 58, 219–242.
- Keller, G.H., Richards, A.F., 1967. Sediments of the Malacca Strait, southeast Asia. *J. Sediment. Petrol.* 37, 102–127.
- Keller, G.H., Barron, J.A., 1983. Paleoceanographic implications of Miocene deep-sea hiatuses. *Geol. Soc. Am. Bull.* 94, 590–613.
- Keller, G., 1985. Depth stratification of planktonic foraminifers in the Miocene ocean. In: Kennett, J.P. (Ed.), *The Miocene Ocean*, Geological Society of America Memoir, vol. 163, pp. 177–195.
- Kennett, J.P., Keller, G., Srinivasan, M.S., 1985. Miocene planktonic foraminiferal biogeography and paleoceanography development of the Indo-Pacific region. In: Kennett, J.P. (Ed.), *The Miocene Ocean: Paleoceanography and Biogeography*, Geological Society of America Memoirs, vol. 163, pp. 197–236.
- Khan, P.K., Chakraborty, P., 2005. Two-phase opening of Andaman Sea: a new seismotectonic insight. *Earth Planet. Sci. Lett.* 229, 259–271.
- Lee, T., Fukumori, I., Menemenlis, D., Xing, Z., Fu, L.-L., 2002. Effects of the Indonesian Throughflow on the Pacific and Indian Oceans. *J. Phys. Oceanogr.* 32, 1404–1429.
- Leinen, 1979. Biogenic silica accumulation in the central equatorial Pacific and its implications for Cenozoic paleoceanography. *Geol. Soc. Am. Bull.* 90, 1310–1376.
- Lyle, M., Murray, D., Finney, B., Dymond, J., Robbins, J., Brooksforce, K., 1988. The record of Late Pleistocene biogenic sedimentation in the eastern tropical Pacific Ocean. *Paleoceanography* 3, 39–59.
- Madhupratap, M., Gauns, M., Ramaiah, N., Kumar, S.P., Muraleedharan, P.M., de Souza, S.N., Sardessai, S., Muraleedharan, U., 2003. Biogeochemistry of the Bay of Bengal: physical, chemical and primary productivity characteristics of the central and western Bay of Bengal during the summer monsoon 2001. *Deep Sea Res. Part II* 50, 881–896.
- Martin, E.E., Scher, H., 2006. A Nd isotopic study of southern sourced waters and Indonesian Throughflow at intermediate depths in the Cenozoic Indian Ocean. *Geochim. Geophys. Geosyst.* 7, 1–14.
- Martini, E., 1971. Standard tertiary and Quaternary calcareous nannoplankton zonation. In: Farinacci, A. (Ed.), *Proceedings of the 2nd International Conference on Planktonic Microfossils*, vol. 2, pp. 739–785.
- Mucciarone, D., 2003. Biogenic silica analysis procedure. In: Stanford University Stable Isotope Laboratory Standard Operating Procedure Manual. Stanford University Department of Geological and Environmental Sciences, Stanford, CA, pp. 93–105.
- Murthy, V.S.N., Sarma, Y.V.B., Rao, D.P., Murthy, C.S., 1992. Water characteristics, mixing and circulation in the Bay of Bengal during southwest monsoon. *J. Mar. Res.* 50, 207–228.
- Naqvi, W.A., Charles, C.D., Fairbanks, R.G., 1994. Carbon and oxygen records of benthic foraminifera from the Northeast Indian Ocean: implications on glacial-interglacial atmospheric CO₂ changes. *Earth Planet. Sci. Lett.* 121, 99–110.
- Nishimura, S., Suparka, S., 1997. Tectonic approach to the Neogene evolution of Pacific–Indian Ocean seaways. *Tectonophysics* 281, 1–16.
- Okada, H., Bukry, D., 1980. Supplementary modification and introduction of code numbers to the low-latitude coccolith biostratigraphic zonation (Bukry, 1973, 1975). *Mar. Micropaleontol.* 5, 349–379.
- Pal, T., Chakraborty, P., Gupta, T., Singh, C., 2003. Geodynamic evolution of the outer-arc–forearc belt in the Andaman Islands, the central part of the Burma–Java subduction complex. *Geol. Mag.* 140, 289–307.
- Phillips, S.C., Johnson, J.E., Giosan, L., Rose, K., 2014. Monsoon-influenced variation in productivity and lithogenic sediment flux since 110 ka in the offshore Mahanadi Basin, northern Bay of Bengal. *J. Mar. Pet. Geol.*
- Peterson, L.C., 1984. Recent abyssal benthic foraminiferal biofacies of the eastern equatorial Indian Ocean. *Mar. Micropaleontol.* 8, 479–519.
- Peterson, L.C., Murray, D.W., Ehrmann, W.U., Hempel, P., 1992. Cenozoic carbonate accumulation and compensation depth changes in the Indian Ocean. In: Duncan, R.A., Rea, D.K., Kidd, R.B., Von Rad, U., Weissel, J.K. (Eds.), *Synthesis of Results from Scientific Drilling in the Indian Ocean*, American Geophysical Union Geophysical Monograph, vol. 70, pp. 311–333.
- Powell, C.M., Roots, S.R., Veevers, J.J., 1988. Pre-breakup continental extension in East Gondwanaland and the early opening of the eastern Indian Ocean. *Tectonophysics* 155, 261–283.
- Prassana Kumar, S., Muraleedharan, P.M., Prasad, T.G., Gauns, M., Ramaiah, N., de Souza, S.N., Sardesai, S., Madhupratap, M., 2002. Why is the Bay of Bengal less productive during summer monsoon compared to the Arabian Sea? *Geophys. Res. Lett.* 29 <http://dx.doi.org/10.1029/2002GL016013>.
- Raffi, I., Backman, J., Fornaciari, E., Palike, H., Rio, D., Lourens, L., Hilgen, F., 2006. A review of calcareous nannofossil astrobiochronology encompassing the past 25 million years. *Quat. Sci. Rev.* 25, 3113–3137.
- Raffi, I., Flores, J.-A., 1995. Pleistocene through Miocene calcareous nannofossils from eastern equatorial Pacific Ocean (Leg 138). In: Pisias, N.G., Mayer, L.A., Janecek, T.R., Palmer-Julson, A., van Andel, T.H. (Eds.), *Proceedings of the Ocean Drilling Program, Scientific Results*, vol. 138, pp. 233–286.
- Rai, A.K., Singh, V.B., 2012. Response of eastern Indian Ocean (ODP Site 762B) benthic foraminiferal assemblages to the closure of the Indonesian seaway. *Oceanologia* 54, 449–472.
- Raju, K.A., Murty, G., Amarnath, D., Kumar, M., 2007. The west Andaman fault and its influence on the aftershock pattern of the recent megathrust earthquakes in the Andaman–Sumatra region. *Geophys. Res. Lett.* 34, 1–5.
- Raju, K.A., Ramprasad, T., Rao, P., Rao, B., Varghese, J., 2004. New insights into the tectonic evolution of the Andaman basin, northeast Indian Ocean. *Earth Planet. Sci. Lett.* 221, 145–162.

- Rizal, S., Damm, P., Wahid, M.A., Sundermann, J., Ilhamsyah, Y., Iskandar, T., Muhamma, 2012. General circulation in the Malacca Strait and Andaman Sea: a numerical model study. *Am. J. Environ. Sci.* 8, 479–488.
- Rodolfo, K., 1969. Bathymetry and marine geology of the Andaman Basin, and tectonic implications for Southeast Asia. *Geol. Soc. Am. Bull.* 80, 1203–1230.
- Rodolfo, K., 1975. The Irrawaddy Delta: tertiary setting and modern offshore sedimentation. *Deltas: Models Explor.* 339–356.
- Romine, K., Lombardi, G., 1985. Evolution of Pacific circulation in the Miocene: radiolarian evidence from DSDP Site 289. In: Kennett, J.P. (Ed.), *The Miocene Ocean: Paleoceanography and Biogeography*, Geological Society of America Memoirs, vol. 163, pp. 273–290.
- Rose, K.K., Johnson, J.E., Torres, M.E., Hong, W., Giosan, L., Solomon, E.A., Kastner, M., Cawthern, T., Long, P.E., Schaeff, H.T., 2014. Anomalous porosity preservation and preferential accumulation of gas hydrate in the Andaman Accretionary Wedge, NGHP-01 Site 17A. *J. Mar. Pet. Geol.*
- Schmitz, B., 1987. Barium, equatorial high productivity and the northward wandering of the Indian Continent. *Paleoceanography* 2, 63–77.
- Schubert, D.J., Villanueva, J., Calvert, S.E., Cowie, G.L., von Rad, U., Schulz, H., Berner, U., Erlenkeuser, H., 1998. Stable phytoplankton community structure in the Arabian Sea over the past 200,000 years. *Nature* 394, 563–566.
- Sengupta, S., Parekh, A., Chakraborty, S., Ravi Kumar, K., Bose, T., 2013. Vertical variation of oxygen isotopes in the Bay of Bengal and its relationships with water masses. *J. Geophys. Res. Oceans* 118 (12), 6411–6424.
- Sijinkumar, A.V., Nath, B.N., Gupta, M.V.S., 2010. Late Quaternary record of pteropod preservation from the Andaman Sea. *Mar. Geol.* 275, 221–229.
- Strickland, J.D.H., Parsons, T.R., 1972. *A Practical Handbook of Seawater Analysis*, second ed. In: *Bulletin 167 Fisheries Research Board of Canada*, Ottawa.
- Susanto, R.D., Fang, G., Soesilo, I., Zheng, Q., Qiao, F., Wei, Z., Sulistyo, B., 2010. SITE: South China Sea-Indonesian Seas transport/exchange. *EOS Trans.* 30, 261–263.
- Susanto, R.D., Ffield, A., Gordon, A.L., Adi, T.R., 2012. Variability of Indonesian Throughflow within Makassar Strait, 2004–2009. *J. Geophys. Res.* 117, 1–16.
- Tripathy, G.R., Singh, S.K., Bhushan, R., Ramaswamy, V., 2011. Sr-Nd isotope composition of the Bay of Bengal sediments. *Impact Clim. Eros. Himal.* 45, 175–186.
- Tozuka, T., Qu, T., Yamagata, T., 2007. Dramatic impacts of the South China Sea on the Indonesian Throughflow. *Geophys. Res. Lett.* 34, 1–5.
- Valsala, V.K., Ikdea, M., 2007. Pathways and effects of the Indonesian Throughflow water in the Indian Ocean using particle trajectory and tracers in an OGCM. *J. Clim.* 20, 2994–3017.
- Varkey, M.J., Murty, V.S.N., Suryanarayana, A., 1996. Physical oceanography of the Bay of Bengal and Andaman Sea. *Oceanogr. Mar. biol.: An Annu. Rev.* 34, 1–70.
- Vincent, E., 1974. Cenozoic planktonic biostratigraphy and paleoceanography of the tropical western Indian Ocean. *Initial Rep. Deep Sea Drill. Proj.* 24, 1111–1150.
- Wang, R., Li, J., Li, B., 2004. Data report: Late Miocene-Quaternary biogenic opal accumulation at ODP Site 1143, southern South China Sea. In: Prell, W.L., Wang, P., Blum, P., Rea, D.K., Clemens, S.C. (Eds.), *Proceedings of the Ocean Drilling Program, Scientific Results*, vol. 184. Ocean Drilling Program, College Station, TX, pp. 1–12.
- Woodruff, F., 1985. Changes in Miocene deep-sea benthic foraminiferal distribution in the Pacific Ocean: relationship to paleoceanography. *Geol. Soc. Am. Bull.* 143, 131–171.
- Wyrtki, K., 1961. *Physical Oceanography of the Southeast Asian Waters*, first ed. University of California, California, p. 195.
- Zhisheng, A., Kutzbach, J.E., Prell, W.L., Porter, S.C., 2001. Evolution of Asian monsoons and phased uplift of the Himalaya–Tibetan plateau since Late Miocene times. *Lett. Nat.* 411, 62–66.